Hydrostatic pressure and growth-direction magnetic field effects on the exciton states in coupled GaAs–(Ga, Al)As quantum wells

2007 J. Phys.: Condens. Matter 19 256202

(http://iopscience.iop.org/0953-8984/19/25/256202)

IOP PUBLISHING JOURNAL OF PHYSICS: CONDENSED MATTER

J. Phys.: Condens. Matter **19** (2007) 256202 (10pp) doi:10.1088/0953-8984/19/25/256202

Hydrostatic pressure and growth-direction magnetic field effects on the exciton states in coupled GaAs–(Ga, Al)As quantum wells

N Raigoza[1], E Reyes-Gómez[1], C A Duque[1] and L E Oliveira[2]

[1] Instituto de Física, Universidad de Antioquia, AA 1226, Medellín, Colombia
[2] Instituto de Física, Unicamp, CP 6165, Campinas, São Paulo, 13083-970, Brazil

Received 1 March 2007, in final form 2 March 2007
Published 31 May 2007
Online at stacks.iop.org/JPhysCM/19/256202

Abstract

The effects of hydrostatic pressure and growth-direction applied magnetic fields on the exciton dispersion and in-plane effective mass in coupled GaAs–(Ga, Al)As quantum wells are investigated. Calculations for spatially direct and indirect excitons were performed within the variational procedure in the effective-mass and nondegenerate parabolic band approximations and by taking into account the coupling between the exciton centre-of-mass momentum and its internal structure. The pressure coefficient is also obtained as a function of both the hydrostatic pressure and growth-direction applied magnetic field.

1. Introduction

The exciton properties of semiconductors and related materials have been the subject of a considerable amount of work in the last few decades. One of the recent motivations for such studies is the possibility for investigating the exciton properties when the electrons and holes are confined in different regions of the direct space. The spatial separation of the electron and hole leads to a small overlap of the single-particle wavefunctions and to a dramatic suppression of the electron–hole recombination. This fact opens up new possibilities for investigating many interesting phenomena, such as superfluidity [1] and Bose–Einstein condensation [2] of excitons in coupled quantum wells (QWs).

The effects of an applied magnetic field on the exciton states in semiconductor heterostructures have also been widely studied. The magnetic field constitutes an excellent tool for obtaining valuable experimental and theoretical information on the exciton states. Since the pioneering work of Gor'kov and Dzyaloshinskiĭ [3], a great number of experimental and theoretical studies have been devoted to the understanding of the influence of the exciton centre-of-mass (CM) momentum on the exciton properties in the cases of direct and indirect excitons [4–8]. For instance, Paquet *et al* [4] studied a two-dimensional (2D) electron–hole fluid in a strong magnetic field by taking into account the influence of the motion of the particles in the direction perpendicular to the magnetic field. Fritze *et al* [5] discussed how an in-plane magnetic field changes the nature of the exciton by inducing a two-body velocity-dependent

interaction. Butov *et al* [6] and Lozovik *et al* [7] carried out the first measurement of the dispersion of an indirect exciton in a coupled double GaAs−$Ga_{0.67}Al_{0.33}As$ QW heterostructure under an external magnetic field, and demonstrated that the exciton effective mass, which is determined by the coupling between the CM motion and internal structure of the exciton, becomes larger than the sum of the electron and hole masses for high magnetic field values. The same problem was recently considered by using the variational procedure [8], which leads to an analytical expression for the exciton effective mass as a function of the applied magnetic field. Theoretical results were found in fairly good agreement with the experimental measurements reported by Butov [6] and Lozovik [7].

Another topic which is related to semiconductors and semiconductor heterostructures is the study of the hydrostatic pressure effects on the electronic band structure as well as on the properties of impurity and exciton states in QWs, multiple QWs, and superlattices [9–16]. The effects of the hydrostatic pressure modify the semiconductor band structure and lead to changes in the properties of the elementary excitations of these heterostructure systems. For example, Samara [9] investigated the effects of temperature and hydrostatic pressure on the static dielectric constant for a group of crystalline semiconductors. Venkateswaran *et al* [10] reported the pressure dependences, from 0 to 70 kbar, of some of the observed transitions in the photoluminescence (PL) spectra of GaAs–$Ga_{1-x}Al_xAs$ multiple QW heterostructures, and studied the lowest exciton energy transition at 8, 80 and 300 K. PL measurements were also performed on GaAs single QWs as a function of the hydrostatic pressure [11], and related pressure coefficients were found to decrease with decreasing well width. By introducing a phenomenological pressure-dependent confining potential, Elabsy [12] studied the effects of the Γ–X crossover on the donor binding energies in single QWs. Also, Guha *et al* [13] studied the temperature and pressure dependence of type-I and type-II transitions from PL spectra in GaAs–AlAs superlattices. From the experimental measurements, they found the parameters describing the temperature dependence of the excitonic transition energies, and deduced the corresponding broadening of the PL line. The effects of an external electric field and applied hydrostatic pressure on shallow impurity [14] and exciton [15] states in semiconductor heterostructures were also investigated, and the transition energies in QWs were studied by considering the excitonic effects as well as the anisotropy of the valence band [16].

The aim of the present work is to study the effects of the hydrostatic pressure on direct and indirect excitons in coupled GaAs–(Ga, Al)As QWs under magnetic fields applied along the growth direction. By taking into account the coupling between the CM momentum and internal degrees of freedom, we shall investigate how the magnetic field and hydrostatic pressure modify the exciton dispersion and exciton in-plane effective mass. The present study is performed in the framework of the effective-mass and nondegenerate parabolic band approximations and within a variational procedure. The paper is organized as follows. A theoretical analysis for direct and indirect excitons is given in section 2. Section 3 is concerned with the present theoretical results and discussion. Conclusions are given in section 4.

2. Theoretical framework

Here we work within the effective-mass and nondegenerate parabolic band approximations. The exciton Hamiltonian for a semiconductor heterostructure grown along the z axis, and under hydrostatic pressure Π and growth-direction applied magnetic field $\vec{\mathbf{B}}$, is given by [8]

$$\hat{H} = \frac{1}{2m_e(\Pi, T)}\left(\hat{\vec{\mathbf{p}}}_e + \frac{e}{c}\vec{\mathbf{A}}_e\right)^2 + \frac{1}{2m_h(\Pi, T)}\left(\hat{\vec{\mathbf{p}}}_h - \frac{e}{c}\vec{\mathbf{A}}_h\right)^2 + V_e(\Pi, T, z_e) + V_h(\Pi, T, z_h) - \frac{e^2}{\epsilon(\Pi, T)|\vec{\mathbf{r}}_e - \vec{\mathbf{r}}_h|}, \quad (1)$$

where $\hat{\vec{\mathbf{p}}}_{\mathrm{e}}$ and $\hat{\vec{\mathbf{p}}}_{\mathrm{h}}$ are the momentum operators associated with the electron and hole, respectively, $V_{\mathrm{e}}(\Pi, T, z_{\mathrm{e}})$ and $V_{\mathrm{h}}(\Pi, T, z_{\mathrm{h}})$ are the pressure- and temperature-dependent confining potentials for the electron and hole, respectively, and e is the absolute value of the electron charge. $\vec{\mathbf{A}}(\vec{\mathbf{r}})$ is the vector potential associated with the magnetic field, with $\vec{\mathbf{A}}_{\mathrm{e}} = \vec{\mathbf{A}}(\vec{\mathbf{r}}_{\mathrm{e}})$ and $\vec{\mathbf{A}}_{\mathrm{h}} = \vec{\mathbf{A}}(\vec{\mathbf{r}}_{\mathrm{h}})$. The pressure- and temperature-dependent effective masses m_{e} and m_{h} for the electron and hole, respectively, are given by [6, 16, 17]

$$\frac{m_{\mathrm{e}}}{m_0} = \left[1 + E_0\left(\frac{2}{E_{\mathrm{g}}(\Pi, T)} + \frac{1}{E_{\mathrm{g}}(\Pi, T) + \Delta_0}\right)\right]^{-1}, \tag{2}$$

$$\frac{m_{\mathrm{h}}}{m_0} = \frac{m_{\mathrm{h0}}}{m_0} + a_1\Pi + a_2\Pi^2, \tag{3}$$

where m_0 is the free-electron mass, $\frac{m_{\mathrm{h0}}}{m_0} = 0.18$, $E_0 = 7.51$ eV, $\Delta_0 = 0.341$ eV, $a_1 = -0.1 \times 10^{-3}$ kbar^{-1}, $a_2 = 5.56 \times 10^{-6}$ kbar^{-2}, and

$$E_{\mathrm{g}}(\Pi, T) = E_{\mathrm{g}}^0 + \alpha_0\Pi + \beta_0\Pi^2 + b\frac{T^2}{T + c} \tag{4}$$

is the bulk GaAs band gap, where E_{g}^0 is the $T = 0$ and $\Pi = 0$ GaAs energy gap ($E_{\mathrm{g}}^0 = 1.519$ eV) [17]. The above pressure coefficients were taken as $\alpha_0 = 10.7$ meV kbar^{-1} and $\beta_0 = -0.0377$ meV kbar^{-2} for GaAs, and the temperature parameters in equation (4) are chosen as [12] $b = -0.5405$ meV K^{-1} and $c = 204$ K. The low temperature-dependent and pressure-dependent static dielectric constant is evaluated using the expression [9, 16, 18]

$$\epsilon = \epsilon_0 \exp[\delta_1(T - T_0) - \delta_2\Pi], \tag{5}$$

where $\epsilon_0 = 12.74$, $\delta_1 = 9.4 \times 10^{-5}$ K^{-1}, $\delta_2 = 1.67 \times 10^{-3}$ kbar^{-1}, and $T_0 = 75.6$ K. For simplicity, both the electron and hole effective masses as well as the dielectric constant have been considered the same throughout the heterostructure.

Due to the conservation of the in-plane component ($\hat{\vec{\mathbf{P}}}_{\perp}$) of the exciton CM magnetic momentum [3, 8], the $\Psi(\vec{\mathbf{r}}_{\mathrm{e}}, \vec{\mathbf{r}}_{\mathrm{h}})$ exciton envelope wavefunction must simultaneously be an eigenfunction of both $\hat{H}$ and $\hat{\vec{\mathbf{P}}}_{\perp}$ and, therefore, it may be written as [3]

$$\Psi(\vec{\mathbf{r}}_{\mathrm{e}}, \vec{\mathbf{r}}_{\mathrm{h}}) = \exp\left[\frac{\mathrm{i}}{\hbar}\left(\vec{\mathbf{P}}_{\perp} + \frac{e}{2c}\vec{\mathbf{B}} \times \vec{\mathbf{r}}\right) \cdot \vec{\mathbf{R}}\right] \Phi_{\mathbf{P}_{\perp}}(\vec{\boldsymbol{\rho}}, z_{\mathrm{e}}, z_{\mathrm{h}}), \tag{6}$$

where $\vec{\mathbf{r}} = \vec{\mathbf{r}}_{\mathrm{e}} - \vec{\mathbf{r}}_{\mathrm{h}}$ is the internal exciton coordinate, $\vec{\boldsymbol{\rho}} = \vec{\boldsymbol{\rho}}_{\mathrm{e}} - \vec{\boldsymbol{\rho}}_{\mathrm{h}}$ is the in-plane internal exciton coordinate, $\vec{\mathbf{R}}(\Pi, T) = \frac{1}{M}[m_{\mathrm{e}}\vec{\boldsymbol{\rho}}_{\mathrm{e}} + m_{\mathrm{h}}\vec{\boldsymbol{\rho}}_{\mathrm{h}}]$ is the in-plane exciton CM coordinate, and $M(\Pi, T) = m_{\mathrm{e}} + m_{\mathrm{h}}$ is the total exciton mass. Here we have considered the magnetic field applied along the growth direction and taken the symmetric gauge $\vec{\mathbf{A}}(\vec{\mathbf{r}}) = \frac{1}{2}\vec{\mathbf{B}} \times \vec{\mathbf{r}}$ for the vector potential. As we are interested in both direct and indirect exciton states in deep and narrow DQW heterostructures, one may model (cf figure 1) the exciton envelope wavefunction as

$$\Phi_{\mathbf{P}_{\perp}} = \psi_{P_{\perp}}(\vec{\boldsymbol{\rho}})\delta(z - d), \tag{7}$$

which may be shown to satisfy

$$\hat{h}_{2D}\psi_{P_{\perp}}(\vec{\boldsymbol{\rho}}) = E_{\mathrm{X}}\psi_{P_{\perp}}(\vec{\boldsymbol{\rho}}), \tag{8}$$

where

$$\hat{h}_{2D} = \frac{\hat{p}_{\perp}^2}{2\mu} + \frac{e\gamma}{2\mu c}\vec{\mathbf{B}} \cdot (\vec{\boldsymbol{\rho}} \times \hat{\vec{\mathbf{p}}}_{\perp}) + \frac{e^2B^2}{8\mu c^2}\rho^2 + \vec{\mathbf{F}} \cdot \vec{\boldsymbol{\rho}} - \frac{e^2}{\epsilon r} + \frac{P_{\perp}^2}{2M}, \tag{9}$$

E_{X} is the exciton energy, $\mu = \mu(\Pi, T)$ is the exciton reduced mass, $\gamma(\Pi, T) = \frac{m_{\mathrm{h}} - m_{\mathrm{e}}}{M}$, $\hat{\vec{\mathbf{p}}}_{\perp} = -\mathrm{i}\hbar\frac{\partial}{\partial\vec{\boldsymbol{\rho}}}$, $\vec{\mathbf{F}} = \frac{e}{Mc}\vec{\mathbf{P}}_{\perp} \times \vec{\mathbf{B}}$, $r = \sqrt{\rho^2 + d^2}$, and we take $P_Z = 0$ due to the strong

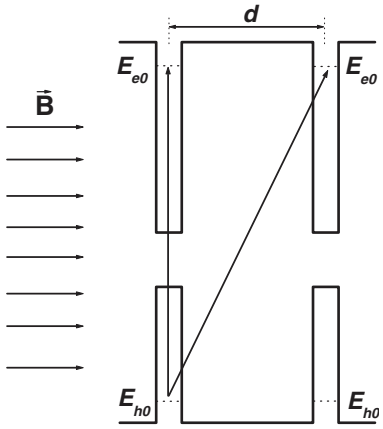

Figure 1. Schematic view of the e–h transitions giving rise to the direct and indirect excitons in the double-quantum-well model used in the present study; the electron and hole either reside in the same layer (direct exciton) or in layers separated by a distance d (indirect exciton) along the growth direction.

confinement (cf figure 1). Here d is the pressure-dependent distance between the electron and hole planes (of course, the direct exciton state is obtained by taking $d = 0$) and is given by [14]

$$d = d_0[1 - (S_{11} - 2S_{12})\Pi], \tag{10}$$

where d_0 is the distance between the electron and hole planes in the absence of hydrostatic pressure, and S_{11} and S_{12} are the compliance constants [19, 20] of GaAs.

For the exciton ground state, one may choose

$$\psi_{P_\perp}(\vec{\boldsymbol{\rho}}) = N \exp\left[\mathrm{i}\frac{\gamma}{2\hbar}\vec{\boldsymbol{\rho}} \cdot \vec{\mathbf{P}}_\perp - \frac{|\vec{\boldsymbol{\rho}} - \vec{\boldsymbol{\rho}}_0|^2}{4l_\mathrm{B}^2}\right] \mathrm{e}^{-\lambda[\sqrt{\rho^2+d^2}-d]}, \tag{11}$$

where N is a normalization constant, $\vec{\boldsymbol{\rho}}_0 = \frac{c}{eB^2}\vec{\mathbf{B}} \times \vec{\mathbf{P}}_\perp$ corresponds to the separation between the two local minima (one associated with the Coulomb potential and the other with the magnetic parabolic potential) of the effective potential in which the exciton moves [8], $l_\mathrm{B} = \sqrt{\frac{\hbar c}{eB}}$ is the Landau magnetic length (or cyclotron radius), and λ is a variational parameter which may be found through the minimization of the functional

$$E_\mathrm{X}(\lambda) = \frac{\langle\psi_{P_\perp}|\hat{h}_{2D}|\psi_{P_\perp}\rangle}{\langle\psi_{P_\perp}|\psi_{P_\perp}\rangle}. \tag{12}$$

The exciton binding energy may be readily obtained, therefore, as

$$E_\mathrm{B} = \tfrac{1}{2}\hbar\omega_c - E_\mathrm{X}, \tag{13}$$

where $\omega_c = \frac{eB}{\mu(\Pi,T)c}$ is the cyclotron frequency and E_X is the optimized value of the above functional.

3. Results and discussion

Here we note that two different regimes may be established to distinguish the exciton behaviours. As mentioned before, the exciton moves in an effective potential with two local minima separated by the vector [3, 7] $\vec{\boldsymbol{\rho}}_0$. One of those minima corresponds to the Coulomb

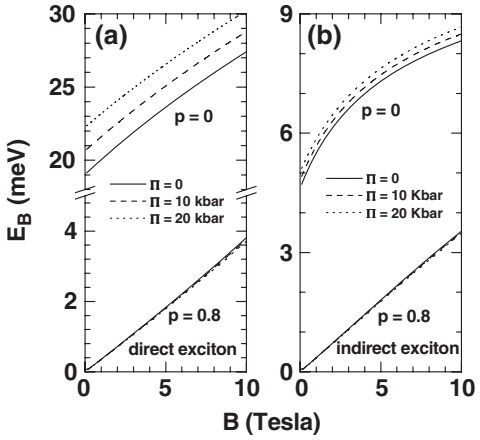

Figure 2. Magnetic field dependence of the exciton binding energy for (a) direct and (b) indirect ($d_0 = 100$ Å) excitons for three different values of the hydrostatic pressure. Results were obtained for two values of the in-plane CM momentum expressed in reduced units, i.e., $p = \frac{P_\perp}{P_0}$, where $P_0 = \frac{e^2 M(\Pi,T)}{\epsilon(\Pi,T)\hbar}$ (see the text).

potential and the other to the magnetic parabolic potential. For $\vec{\mathbf{B}} \neq \vec{\mathbf{0}}$ and $\vec{\mathbf{P}}_\perp = \vec{\mathbf{0}}$ or sufficiently small, the two minima coincide or they are very near, and the exciton properties are established by the magnetic field and the Coulomb potential. This is the so-called hydrogen-like regime. On the other hand, as $P_\perp = |\vec{\mathbf{P}}_\perp| \to \infty$, $|\vec{\boldsymbol{\rho}}_0| \to \infty$, and the properties of the exciton states are essentially determined by the magnetic parabolic potential [3, 7]. In this case it is said that the exciton is in the magnetoexciton regime. The transition between the two regimes takes place at a certain value $P_{\rm tr}$ of the in-plane CM momentum, which is a function both of the growth-direction applied magnetic field and hydrostatic pressure. For sufficiently large values of $P_\perp$, the electron–hole pair becomes more and more polarized due to the increasing Lorentz force acting separately upon the electron and hole. As a consequence, the Coulomb attraction between the electron and the hole becomes less important, and the exciton binding energy tends towards zero. The exciton then behaves as a free and uncorrelated electron–hole system whose total energy is the sum of the lowest electron and hole Landau-level energies. On the other hand, for small values of the CM momentum, the effects of the Lorentz force over the electron–hole pair are weak and the exciton is in the hydrogen-like regime.

In figure 2 we display the exciton binding energy as a function of the applied magnetic field for two values of p, where $p = \frac{P_\perp}{P_0}$ is the in-plane CM momentum in units of $P_0 = \frac{e^2 M(\Pi,T)}{\epsilon(\Pi,T)\hbar}$, for $T = 1.8$ K. Solid, dashed, and dotted lines correspond to hydrostatic pressure values of 0, 10 kbar and 20 kbar, respectively. Figures 2(a) and (b) correspond to the direct and the indirect (with $d_0 = 100$ Å) excitons, respectively. In the zero-CM-momentum limit [6] the exciton binding energy depends on the magnetic field as $\sqrt{B}$. However, when $P_\perp > P_{\rm tr}$ an abrupt change on this dependence is observed, and for sufficiently large values of $P_\perp$ the exciton binding energy transforms into a linear function of B. One may note that the hydrostatic pressure effects are more visible in the hydrogen-like regime than in the magnetoexciton regime.

The hydrostatic pressure dependence of the exciton binding energy is displayed in figure 3 for various values of the applied magnetic field and for $T = 1.8$ K. Results shown in figures 3(a) and (b) correspond to $p = 0$ and $p = 1$, respectively. Solid and dashed lines are the theoretical results for direct and indirect (with $d_0 = 100$ Å) excitons, respectively. For given

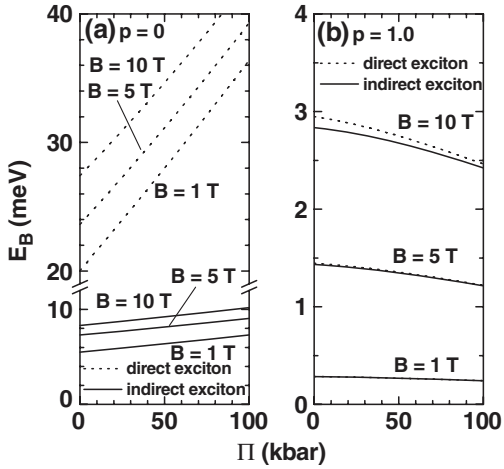

Figure 3. Exciton binding energies as functions of the hydrostatic pressure for (a) $p = 0$ and (b) $p = 1$, respectively, where p is the in-plane CM momentum in reduced units. Calculations are performed for direct (dotted curves) and indirect (full curves; $d_0 = 100$ Å) excitons and for three different values of the growth-direction applied magnetic field.

values of the magnetic field and CM momentum, as the hydrostatic pressure increases, there are two competitive effects determining the exciton behaviour. On one hand, the dielectric constant decreases as the pressure is increased, leading to an increase in the Coulomb interaction and exciton wavefunction confinement, and therefore in the exciton binding energy. On the other hand, the electron and hole masses as well as the exciton reduced effective mass increase as the pressure is increased, leading to an increase in the confinement of the single-particle electron and hole wavefunctions and to a decrease in the e–h overlap, which leads to a decreasing exciton binding energy. In the hydrogen-like regime the contribution of the Coulomb potential to the exciton binding energy is more important, and E_{B} behaves as an increasing function of the hydrostatic pressure. In the magnetoexciton regime, however, the Coulomb interaction is small, and the exciton behaves like two uncorrelated particles (electron and hole), with a decreasing binding energy as a function of the hydrostatic pressure. Therefore, the effects of the hydrostatic pressure result in an increasing binding energy as a function of the pressure in the hydrogen-like regime ($p = 0$), whereas in the magnetoexciton regime ($p = 1$) the exciton binding energy decreases slowly as the pressure is increased.

The exciton-peak energy (or the exciton energy measured with respect to the top of the valence band) is also modified by the effects of the hydrostatic pressure and growth-direction applied magnetic field. For given values of the temperature, in-plane CM momentum and applied magnetic field, and for low values of Π, one may fit the exciton-peak energy as a linear function of the hydrostatic pressure, i.e.,

$$E_{\mathrm{X}}(\vec{\mathbf{P}}, \Pi, T, B) = E_{\mathrm{X}}(\vec{\mathbf{P}}, 0, T, B) + \alpha(\vec{\mathbf{P}}, T, B)\Pi, \tag{14}$$

where α is the pressure coefficient which is a function of the in-plane CM momentum as well as of the magnetic field and temperature. Figure 4 displays the pressure coefficient α as a function both of the in-plane CM momentum (figures 4(a) and (c)) and of the applied magnetic field (figures 4(b) and (d)). Calculations in figures 4(a) and (b) were performed for direct excitons, whereas in figures 4(c) and (d) we have displayed our theoretical results for indirect excitons with $d_0 = 100$ Å. The magnetoexciton and hydrogen-like regimes are clearly distinguished. In the magnetoexciton regime, the Coulomb interaction between

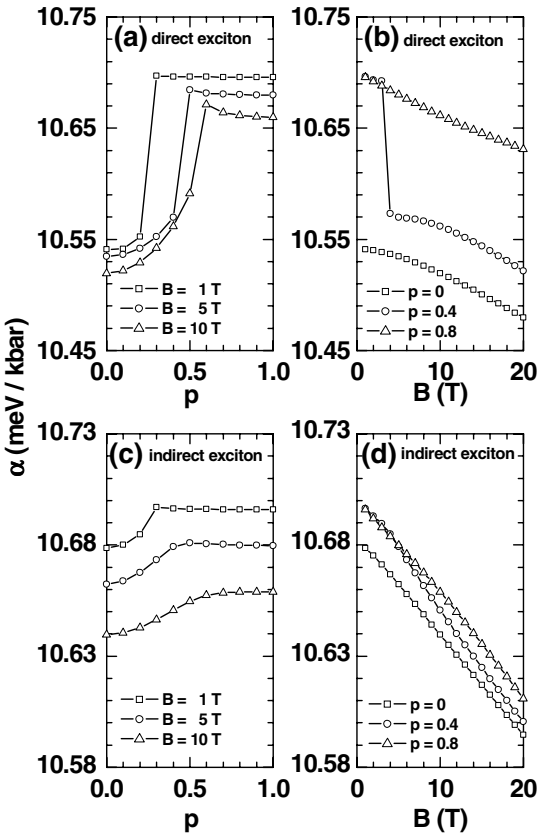

Figure 4. Pressure coefficient α ((a) and (c)) as a function of the in-plane CM momentum expressed in reduced units for three different values of the applied magnetic field, and ((b) and (d)) as a function of the magnetic field for three different values of the in-plane CM momentum. Results displayed in (a) and (b) correspond to direct excitons, whereas calculations shown in (c) and (d) are for indirect excitons.

the electron and hole is negligible, and the pressure-dependent exciton energy is essentially the sum of the lowest electron and hole Landau-level energies including the GaAs band-gap energy. Therefore, for a fixed value of the magnetic field in the magnetoexciton regime, the pressure coefficient depends weakly on the CM momentum, as one may see from figures 4(a) and (c) for the higher values of p. In addition, for a small value of the magnetic field, α tends towards α_0 in the magnetoexciton regime (cf equation (4)), as expected. In the hydrogen-like regime, however, the Coulomb interaction plays a relevant role in the exciton behaviour, leading to a coefficient α slightly smaller than α_0. For all values of the CM momentum used in our calculations, it is apparent from figures 4(b) and (d) that the pressure coefficient α is a decreasing function of the magnetic field. For $p = 0$ the exciton remains in the hydrogen-like regime in the range of magnetic field values considered here, whereas for $p = 0.8$ the exciton is in the magnetoexciton regime for all values of B. For intermediate values of the in-plane CM momentum ($p = 0.4$), a transition from the magnetoexciton regime to the hydrogen-like regime takes place (cf figures 4(b) and (d)). Such a transition is more remarkable in the case of direct excitons, as one may see from figure 4(b).

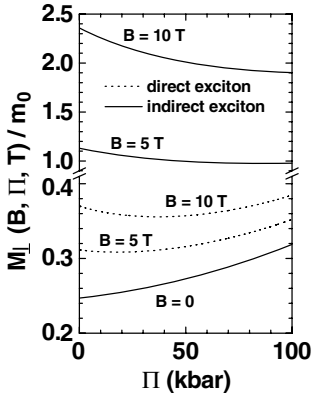

Figure 5. In-plane exciton effective mass $M_\perp(B, \Pi, T)$, where m_0 is the free-electron mass, as a function of the hydrostatic pressure for direct (dotted curves) and indirect (full curves; $d_0 = 115$ Å) excitons and for three different values of the growth-direction applied magnetic field.

As shown in previous work [8], the exciton energy may be expressed, near $\vec{\mathbf{P}} = \vec{\mathbf{0}}$, as

$$E_{\mathrm{X}}(\vec{\mathbf{P}}, \Pi, T, B) = E_{\mathrm{X}}(\vec{\mathbf{0}}, \Pi, T, B) + \tfrac{1}{2}(P_x, P_y, P_z)\mathbb{M}_{\mathrm{X}}^{-1}\begin{pmatrix} P_x \\ P_y \\ P_z \end{pmatrix}, \tag{15}$$

where

$$\mathbb{M}_{\mathrm{X}}^{-1} = \begin{pmatrix} M_\perp^{-1} & 0 & 0 \\ 0 & M_\perp^{-1} & 0 \\ 0 & 0 & M^{-1} \end{pmatrix} \tag{16}$$

is the inverse of the anisotropic exciton mass, and

$$M_\perp(\Pi, T, B) = \frac{M(\Pi, T)}{1 - \frac{\langle\rho^2\rangle_0}{2l_{\mathrm{B}}^2}} \tag{17}$$

is the in-plane exciton mass, with

$$\langle\rho^2\rangle_0 = \langle\Phi_{P_\perp}|\rho^2|\Phi_{P_\perp}\rangle|_{\vec{\mathbf{P}}_\perp = \vec{\mathbf{0}}}. \tag{18}$$

We have then calculated the in-plane exciton effective mass $M_\perp(B, \Pi, T)$, at $T = 1.8$ K, as a function of the hydrostatic pressure and for different values of the growth-direction applied magnetic field. Results are displayed in figure 5 for both direct and indirect ($d_0 = 115$ Å) excitons. For $B = 0$, the in-plane exciton mass has the same value for direct and indirect excitons (cf equation (17)) and is a growing function of the hydrostatic pressure, as one may expect from equations (2) and (3). For $B = 5$ and 10 T and for direct excitons, the in-plane exciton mass decreases as the pressure is increased until it reaches a local minimum, and then it increases as the pressure increases. In the indirect exciton case, however, the in-plane exciton mass under finite values of the applied magnetic field is a decreasing function over the whole range of the pressure considered in the present calculations.

We have also calculated the in-plane exciton mass as a function of the applied magnetic field for $T = 1.8$ K. Results are shown in figure 6 for $\Pi = 0$ and 100 kbar for direct and indirect ($d_0 = 115$ Å) excitons. Open circles in figure 6 are the experimental data obtained by Butov *et al* and Lozovik *et al* [6, 7] for an indirect exciton in a GaAs–$Ga_{0.67}Al_{0.33}As$ double-coupled QW with $d_0 = 115$ Å at $T = 1.8$ K. One may see that the exciton in-plane effective mass increases as the magnetic field is increased. For indirect excitons, the effects of the hydrostatic

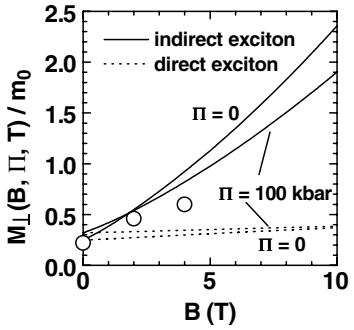

Figure 6. In-plane exciton effective mass $M_{\perp}(B, \Pi, T)$, where m_0 is the free-electron mass, as a function of the growth-direction applied magnetic field for direct (dotted curves) and indirect (full curves; $d_0 = 115$ Å) excitons, and for applied hydrostatic pressure $\Pi = 0$ and 100 kbar. Open circles correspond to the experimental results from Butov *et al* [6] and Lozovik *et al* [7] in $\Pi = 0$ coupled GaAs–$Ga_{0.67}Al_{0.33}As$ QWs.

pressure result in a small increase of the exciton in-plane mass for the lowest fields, and in a weak decrease of the in-plane mass for the largest values of the magnetic field used in the calculations, whereas for direct excitons, effects of both the applied hydrostatic pressure and growth-direction magnetic field are quite small. Here we note that the discrepancy between calculated results for indirect excitons and experimental measurements can probably be solved by including the effects of the double-coupled QW confining potential in the model calculation. Moreover, results for the pressure-dependent and magnetic field-dependent exciton in-plane effective mass may find applications in phenomena such as the Bose–Einstein condensation [2], as it is well known that the condensation temperature of the bosonic gas depends on the inverse of the boson mass. In the case of the excitons, because of the exciton-mass values, the critical temperature [2] at which condensation take places is about 1 K, and, therefore, the present calculations indicate that, by modifying the magnetic field and/or the hydrostatic pressure, the condensation temperature of the exciton gas may be modified together with the exciton effective mass in the semiconductor heterostructure.

4. Conclusions

In summary, we have studied the effects of hydrostatic pressure on the exciton properties of coupled GaAs–(Ga, Al)As QWs under magnetic fields applied along the growth direction. We have clearly observed the transition between the hydrogen-like and magnetoexciton regimes from the magnetic field dependence of the exciton binding energy. Such a transition is also observable in the behaviour of the pressure coefficients as functions of the applied magnetic field as well as of the in-plane CM momentum, and it is more remarkable for direct excitons.

In addition, we have investigated the effects of both the hydrostatic pressure and magnetic fields on the exciton effective mass on spatially direct and indirect excitons in coupled GaAs–(Ga, Al)As QWs. We have shown that the magnetic field effects on the exciton in-plane effective mass are stronger than the effects due to the hydrostatic pressure and suggested that the present theoretical results may have implications for the values of the condensation temperature of the two-dimensional exciton gas in semiconductor heterostructures.

Acknowledgments

The authors would like to thank the Colombian COLCIENCIAS Agency, CODI-Universidad de Antioquia, and Brazilian Agencies CNPq, FAPESP, MCT-Millennium Institute of Quantum

Information, and MCT-Millennium Institute of Nanotechnology for partial financial support. This work was also partially financed by the Excellence Centre for Novel Materials and COLCIENCIAS under contract No 043-2005. LEO wishes to thank for warm hospitality the Instituto de Física of the Universidad de Antioquia, Medellín, Colombia, where part of this work was performed.

References

[1] Lozovik Yu E, Berman O L and Willander M 2002 *J. Phys.: Condens. Matter* **14** 12457
[2] Butov L V, Lai C W, Ivanov A L, Gossard A C and Chemla D S 2002 *Nature* **417** 47
[3] Gor'kov L P and Dzyaloshinskiĭ I E 1968 *Sov. Phys.—JETP* **26** 449
[4] Paquet D, Rice T M and Ueda K 1985 *Phys. Rev.* B **32** 5208
[5] Fritze M, Perakis I E, Getter A, Knox W, Goosen K W, Cunningham J E and Jackson S A 1996 *Phys. Rev. Lett.* **76** 106
[6] Butov L V, Lai C W, Chemla D S, Lozovik Yu E, Campman K L and Gossard A C 2001 *Phys. Rev. Lett.* **87** 216804
[7] Lozovik Yu E, Ovchinnikov I V, Volkov S Yu, Butov L V and Chemla D S 2002 *Phys. Rev.* B **65** 235304
[8] Reyes-Gómez E, Oliveira L E and de Dios-Leyva M 2005 *Phys. Rev.* B **71** 045316
Reyes-Gómez E, Oliveira L E and de Dios-Leyva M 2005 *Phys. Status Solidi* b **242** 1829
[9] Samara G A 1983 *Phys. Rev.* B **27** 3494
[10] Venkateswaran U, Chandrasekhar M, Chandrasekhar H R, Wolfram T, Ficher R, Masselink W T and Morkoç H 1985 *Phys. Rev.* B **31** 4106
[11] Venkateswaran U, Chandrasekhar M, Chandrasekhar H R, Bojak B A, Chambers F A and Meese J M 1986 *Phys. Rev.* B **33** 8416
[12] Elabsy A M 1994 *J. Phys.: Condens. Matter* **6** 10025
[13] Guha S, Cai Q, Chandrasekas M, Chandrasekar H R, Kim H, Alvarenga A D, Vogelgesang R, Rambas A K and Melloch M R 1998 *Phys. Rev.* B **58** 7222
[14] Morales A L, Montes A, López S Y and Duque C A 2002 *J. Phys.: Condens. Matter* **14** 987
[15] Raigoza N, Duque C A, Reyes-Gómez E and Oliveira L E 2005 *Physica* B **367** 267
[16] Raigoza N, Duque C A, Reyes-Gómez E and Oliveira L E 2006 *Phys. Status Solidi* b **243** 635
[17] Herbert Li E 2000 *Physica* E **5** 215
[18] Kopf R F, Herman M H, Lamont Schones M, Perley A P, Livescu G and Ohring M 1992 *J. Appl. Phys.* **71** 5004
[19] Aspnes D E 1976 *Phys. Rev.* B **14** 5331
[20] Yu P Y and Cardona M 1998 *Fundamentals of Semiconductors* (Berlin: Springer)